Current Biology

Article

A Reservoir of Pluripotent Phloem Cells Safeguards the Linear Developmental Trajectory of Protophloem Sieve Elements

Graphical Abstract

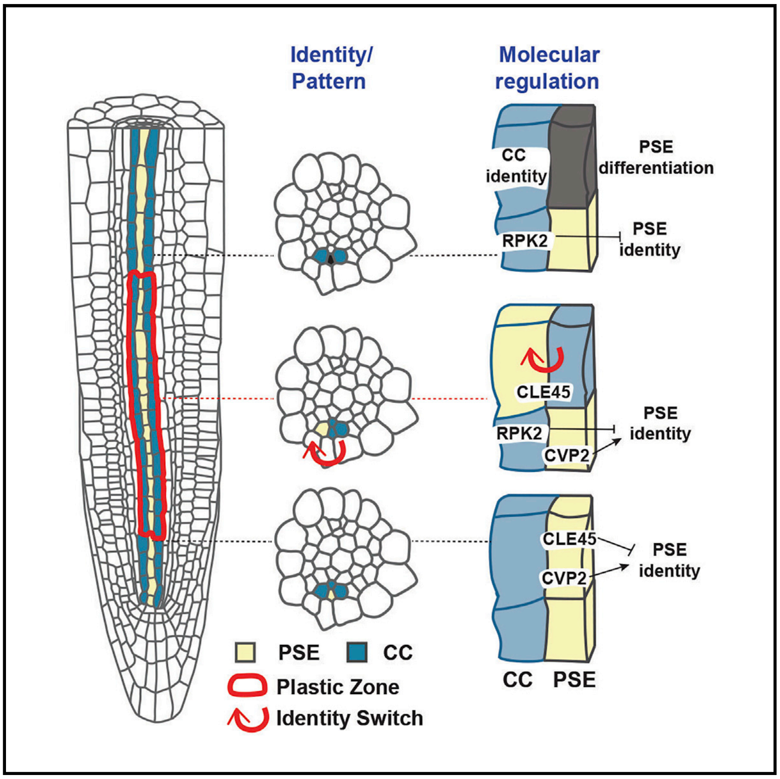

Highlights

- An early PSE misspecification promotes identity hybridism between PSE and CC
- Meristematic CC and MSE retain plastic identity to safeguard phloem functionality
- RPK2 excludes PSE identity from PSE-surrounding cells within the root meristem
- CLE45 maintains PSE and PSE-surrounding cells in a plastic identity stage

Authors

Bojan Gujas, Elizabeth Kastanaki, Alessandra Sturchler, ..., Simona Eicke, Elisabeth Truernit, Antia Rodriguez-Villalon

Correspondence

antia.rodriguez@ethz.ch

In Brief

Gujas et al. describe a molecular mechanism that endows plant cells with a plastic cell fate. Hereby, CLE-RPK2 module halts heterogeneous phloem cells sub-specification. This plastic identity state safeguards the re-establishment of a functional phloem pattern in case conductive protophloem fails to form in its by-lineage-predestined position.

Gujas et al., 2020, Current Biology *30*, 755–766

https://doi.org/10.1016/j.cub.2019.12.043

CellPress

Current Biology
Article

A Reservoir of Pluripotent Phloem Cells Safeguards the Linear Developmental Trajectory of Protophloem Sieve Elements

Bojan Gujas,[1,4] Elizabeth Kastanaki,[1,4] Alessandra Sturchler,[1] Tiago M.D. Cruz,[1] M. Aguila Ruiz-Sola,[2] Rene Dreos,[3] Simona Eicke,[2] Elisabeth Truernit,[2] and Antia Rodriguez-Villalon[1,5,*]
[1]Group of Plant Vascular Development, Swiss Federal Institute of Technology (ETH) Zurich, 8092 Zurich, Switzerland
[2]Group of Phloem Development, Swiss Federal Institute of Technology (ETH) Zurich, 8092 Zurich, Switzerland
[3]Group of NCCR RNA and Disease, University of Lausanne, 1015 Lausanne, Switzerland
[4]These authors contributed equally
[5]Lead Contact
*Correspondence: antia.rodriguez@ethz.ch
https://doi.org/10.1016/j.cub.2019.12.043

SUMMARY

Plant cells can change their identity based on positional information, a mechanism that confers developmental plasticity to plants. This ability, common to distinct multicellular organisms, is particularly relevant for plant phloem cells. Protophloem sieve elements (PSEs), one type of phloem conductive cells, act as the main organizers of the phloem pole, which comprises four distinct cell files organized in a conserved pattern. Here, we report how *Arabidopsis* roots generate a reservoir of meristematic phloem cells competent to swap their cell identities. Although PSE misspecification induces cell identity hybridism, the activity of *RECEPTOR LIKE PROTEIN KINASE 2* (*RPK2*) by perceiving CLE45 peptide contributes to restrict PSE identity to the PSE position. By maintaining a spatiotemporal window when PSE and PSE-adjacent cells' identities are interchangeable, CLE45 signaling endows phloem cells with the competence to re-pattern a functional phloem pole when protophloem fails to form.

INTRODUCTION

Classical *in vitro* studies have demonstrated the ability of plant cells committed to a certain cell lineage in reprogramming their cell identity [1, 2]. Contrary to animal cells, whose identity is mainly cell-lineage determined, the fate of plant cells is mostly directed by positional information. In *Arabidopsis thaliana* (*Arabidopsis*) root-excised seedlings, cells in the remaining stump can reprogram their cell identities to regenerate the missing organ [1]. With the exception of very few examples, the underlying molecular mechanisms of the plasticity of cell identity are poorly understood. Yet these studies have demonstrated that root cells do not always follow linear developmental trajectories, by which cells undergo a genetically programmed and irreversible path toward a terminal cell fate. This scenario is reflected in the conversion of phloem cells into conductive units [3]. In *Arabidopsis* roots, the phloem tissues are organized in a conserved pattern comprising four distinct cell file types (Figure 1A). The conductive units, protophloem and metaphloem sieve elements (PSEs and MSEs, respectively), originate from a common stem cell [3, 4]. However, the companion cell (CC) lineage appears to originate from a different daughter cell, which follows a poorly described developmental trajectory to eventually establish two PSE-adjacent cells [3, 5]. The PSEs act as a radial organizer within the phloem pole by controlling the periclinal division rate of its neighboring tissues [5]. Compared to other root cell types, PSEs differentiate closest to the root meristem. This is essential for unloading photoassimilates and growth factors to the growing root apical meristem, assisted by CCs or the adjacent phloem pole pericycle (PPP) cells [6, 7]. To become conductive elements, PSEs undergo a complex differentiation program, which involves cell wall reinforcement and selective organelle dismantling [8]. Suppression of PSE formation by the exogenous application of CLAVATA/EMBRYO SURROUNDING REGION 45 (CLE45) peptide correlates with the impaired development of CCs [4, 9]. The activity of the protophloem-specific CLE45 peptide appears to be required to maintain PSE precursor cells in a meristematic state via its interaction with BARELY ANY MERISTEM 3 (BAM3) [4]. Genetic studies have suggested that the activity of the CLE45-BAM3 signaling module is counteracted by *OCTOPUS* (*OPS*) and *BREVIS RADIX* (*BRX*), two plasma-membrane-associated proteins promoting PSE differentiation [4, 10]. Two protophloem phosphatidylinositol 5-phosphatases, *COTYLEDON VASCULAR PATTERN 2* (*CVP2*) and its homologous *CVP2-LIKE 1* (*CVL1*), are integral in PSE development, because *cvp2 cvl1* PSE cell files in roots exhibit undifferentiated cells, named gap cells, flanked by mature PSE [11]. The latter suggests that tightly balanced phosphatidylinositol-4,5-bisphosphate (PtdIns(4,5)P_2) levels are essential for proper protophloem differentiation [11]. In fact, *cvp2 cvl1*-differentiating PSEs (as evident by their thick cell wall, the first hallmark of PSE differentiation) contained atypical big vacuoles, carrying CELLULOSE SYNTHASE 6 (CESA6), a subunit responsible for primary cell wall formation and for which abundance at the PM depends on membrane trafficking [12]. Moreover, the absence of CC formation or a disturbed CC functionality can be observed in mutants in which sieve element formation is severely affected, such as *ops ops-like 2* or *cvp2 cvl1* [11, 13]. These observations suggest that the developmental trajectories of the PSE and

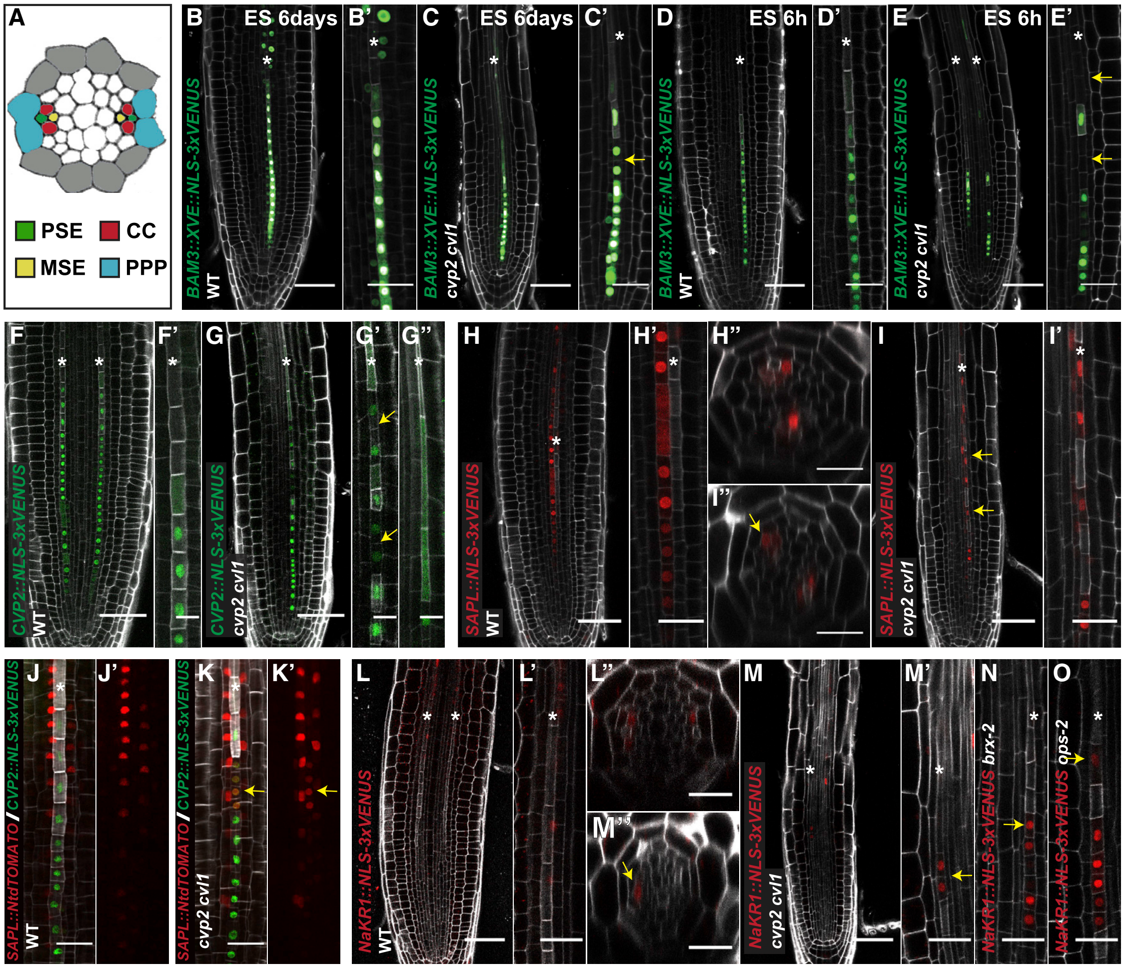

Figure 1. PSEs in *cvp2 cvl1* Roots Exhibit PSE- and CC-Associated Transcripts

(A) The radial organization of the vascular tissues in *Arabidopsis* roots where depicted phloem tissues are color coded (CC, companion cell; MSE, metaphloem sieve element; PPP, protophloem pole pericycle cells; PSE, protophloem sieve element).

(B–E') Absence of *BAM3* expression in *cvp2 cvl1* gap cells when plants were transferred to a medium supplemented with 1 μM estradiol (ES) for 6 h as revealed by confocal microscopy analysis of *BAM3::XVE::NLS-3×VENUS* seedlings. Note the continuous *BAM3* expression in wild-type (WT) as well as in *cvp2 cvl1* protophloem strands when plants were grown for 6 days in ES-supplemented media.

(F–G'') Confocal microscopy analysis of *CVP2* expression in WT and *cvp2 cvl1* roots. A weaker expression of *CVP2* could be observed in the gap cells in comparison to the flanking cell. *CVP2* diffuse expression can be detected in mature PSE cells in *cvp2 cvl1* showing a delay in cytosol dilution.

(H–I'') *SAPL* expression in WT (H–H'', PSE-surrounding cells) and *cvp2 cvl1* (I–I'', PSE-surrounding cells and gap cells [yellow arrow]) roots.

(J–K') Overlapping expression of *SAPL* and the protophloem-specific *CVP2* in PSEs of *cvp2 cvl1* roots.

(L–O) Expression of the CC-specific *NaKR1* gene in gap cells of the indicated genotypes.

White asterisks mark protophloem strands. Yellow arrows indicate gap cells. Scale bars in (B)–(I), (L), and (M) represent 50 μm; otherwise, 20 μm. See also Figure S1 and Table S1.

its adjacent CCs can be closely intertwined. However, it is unclear how similar, if at all, the genetic circuits governing the developmental trajectories of both cell lineages are. Here, we report how PSE misspecification alters the developmental trajectories of PSE-surrounding cells. We demonstrate that the activity of *RECEPTOR PROTEIN LIKE KINASE 2* (*RPK2*) is necessary to repress the lateral expansion of PSE identity, confining it to the PSE position. By combining gene expression profiling with genetic analysis, we show that immature phloem cells retain the ability to change their cell fate before the onset of PSE differentiation to re-pattern a functional phloem pole in case of vascular disruption. Additionally, the perception of the protophloem-specific CLE45 peptide by RPK2 contributes to maintain PSE and its surrounding cells in a phloem pluripotent developmental stage. By modulating the perception of CLE45 at the single cell level, the root can create a local reservoir of phloem cells that can switch their cell fate upon positional cues.

RESULTS

cvp2 cvl1 PSEs Can Exhibit CC Identity Prior to Their Differentiation

To determine the potential plasticity of phloem development, we analyzed the developmental trajectories of phloem cells when the continuous progression of PSE development is severely compromised. This scenario is reflected in *cvp2 cvl1*, which exhibits gap cells in its PSE files [11, 12]. Analysis of *cvp2 cvl1* roots harboring *BAM3::XVE::NLSx-3VENUS*—an estradiol-inducible protophloem marker—demonstrated that gap cells express protophloem -associated genes, such as *BAM3*, when continuously grown in a media supplemented with estradiol (Figures 1B–1C'). Conversely, *BAM3* expression was not detected in gap cells of *cvp2 cvl1* roots when plants were subjected to a shorter estradiol treatment, even if this gene was expressed in all PSEs of wild-type plants (Figures 1D–1E'). These findings suggest that gap cells have ceased or weakened the expression of certain genetic signatures associated to PSE identity. Indeed, *CVP2* expression in *cvp2 cvl1* gap cells was on average 52.47% (±3.68 SE) attenuated in comparison to the nearest protophloem thick-cell-walled cell with signal (Figures 1F–1G'). To further investigate the developmental stage of gap cells, we examined the reconstruction of 3D representations from ultrathin sections generated through serial block face scanning electron microscopy (SBFSEM). Contrary to wild-type, where the disintegration of the nucleus perfectly matches with the completion of PSE differentiation (Figure S1A; cell no. 3), an interrupted differentiation process was observed in *cvp2 cvl1* roots (Figure S1A). Surprisingly, the first differentiated PSE cell, as judged by its thick cell wall and nuclear absence, showed preserved vacuolar-like structures (VLS), a phenotype never observed in wild-type plants (Figure S1B; cell no. 2). Gap cells of *cvp2 cvl1* (Figure S1B; cells no. 3 and no. 4) exhibited intact organelles, including the nucleus. Interestingly, a delay in cell clearance can also be observed in mature thick-cell-walled PSEs in *cvp2 cvl1* (Figure 1G'') [12]. Collectively, these results suggest that PSEs in *cvp2 cvl1* have undergone an incomplete differentiation process. The persistence of VLS in PSEs, a feature observed in PSE-surrounding elements, prompted us to further investigate the genetic identity of PSEs in *cvp2 cvl1* roots. To this end, we isolated developing PSEs based on their expression of the protophloem-specific *CVP2::NLS-3XVENUS* marker, whose expression extends from early PSE proliferation to enucleation (Figures 1F–1G'') [4]. The transcriptional analysis of sorted cells from *cvp2 cvl1* and wild-type plants revealed a set of genes that are highly expressed in the mutant yet barely detectable in wild-type PSEs (Table S1), some of which were proposed to be expressed in CCs (Figure S1C) [7, 9, 14–23]. Upregulation of selected genes was independently confirmed by qPCR (Figure S1C; Table S1). Among others, the transcription factor *SISTER OF APL* (*SAPL*), the closest homolog to *ALTERED PHLOEM DEVELOPMENT* [5, 7], was greatly induced in *cvp2 cvl1* PSEs in comparison to wild-type (Figure S1C). *SAPL* expression is actually excluded from PSEs but expressed in PSE-surrounding cells in wild-type roots (Figures 1H–1H''). However, in *cvp2 cvl1* roots, *SAPL* expression was detected not only in the gap cells but also in some differentiating PSEs (Figures 1I–1I'', S1D, and S1E). Moreover, co-expression of *SAPL::NtdTOMATO* and *CVP2::NLS-3×VENUS* in *cvp2 cvl1* roots showed PSEs in which both genes were simultaneously expressed (Figures 1J–1K'). These findings indicate that gap cells display a hybrid identity, composed of PSE and PSE-surrounding cells' transcripts. To further narrow down this hybrid identity, we analyzed the expression pattern of one of the few known CC-specific marker genes—*SODIUM POTASIUM ROOT DEFECTIVE 1* (*NaKR1*)—in *cvp2 cvl1* roots [24]. The onset of *NaKR1* expression can rarely be detected before the transition zone in wild-type roots, a region where the maturation of CCs occurs (Figure S1G). Yet confocal microscopy analysis demonstrated *NaKR1* expression in mature (after transition zone) and younger gap cells of *cvp2 cvl1* roots (Figures 1L–1M'', S1G, and S1H). Similar gene-expression profiles were found in other protophloem gap-cell-containing mutants, such as *brx-2* and *ops-2* (Figures 1N and 1O). This phenomenon translates in distinct phenotypes in *cvp2 cvl1*, ranging from cells with exclusively PSE traits (exhibiting a partial or total differentiation), to cells that express transcripts associated to mature CCs. Together, these results demonstrate the non-linear developmental trajectory of PSEs in the presented mutants. This altered developmental path results in cell identity hybridism of two cell types normally organized in distinct cell files, a process that most likely occurred in earlier stages of their ontogenesis.

PSE-Surrounding Cells Can Reprogram Their Identity to Re-pattern the Phloem Pole

The hybrid PSE/CC-transcriptome of *cvp2 cvl1* PSEs suggests that their identity can transit between two distinct phloem cell lineages. Thus, it appears plausible that this hybrid identity leads to newly formed CCs at the PSE position. To explore the consequences on other phloem cells upon this identity change, we altered phloem formation by incubating seedlings in brefeldin A (BFA). As a widely used drug to alter vesicle trafficking, BFA inhibits ADP-ribosylation factor-guanine-exchange factors [25]. Previous studies have reported the ability of this compound to generate gap cells in the protophloem strand within 24–48 h treatments [12, 26], although the underlying mechanisms remain unknown. Remarkably, BFA-triggered gap cells also exhibit *SAPL* and *NaKR1* expression (Figures S1F and S1I), mimicking the *cvp2 cvl1* phenotype. BFA-treated roots harboring both *SAPL::NtdTOMATO* and *BAM3::XVE::NLS-3×VENUS* often showed a swapped expression of both genes between PSE and PSE-adjacent cell files (Figures 2A–2D). Notably, identity swapping is mainly observed in newly formed cells (i.e., the proliferating cells before PSE cell wall thickening). Interestingly, a careful examination of *BAM3::XVE::NLS-3×VENUS* upon prolonged estradiol induction showed occasional presence of this gene at the CC position in wild-type roots (Figures 2E–2F'). This phenomenon was enhanced in the *cvp2 cvl1* genetic background, where *BAM3* expression appears in close proximity to the gap cells (Figures 2G and 2G'). BFA effects were enhanced in a *cvp2 cvl1* genetic background, where, in addition to higher gap frequency (Figures 2I and 2J), newly specified PSEs in CC positions start to differentiate, as manifested by their morphology and *BAM3* expression (Figures 2D and 2G–2H'). Collectively, these observations suggest a potential of proliferating phloem cells to commit to a developmental trajectory distinct from their original cell lineage. Because PSEs act as the main organizer of the early phloem pole [5], it is plausible that a compromised PSE formation triggers the activation of this re-patterning mechanism. To test this hypothesis, we eliminated one proliferating PSE cell by laser ablation and followed the behavior of the PSE-surrounding cells. In particular, one of the 5th to 8th PSE cells harboring *CVP2::NLS-3×VENUS* in

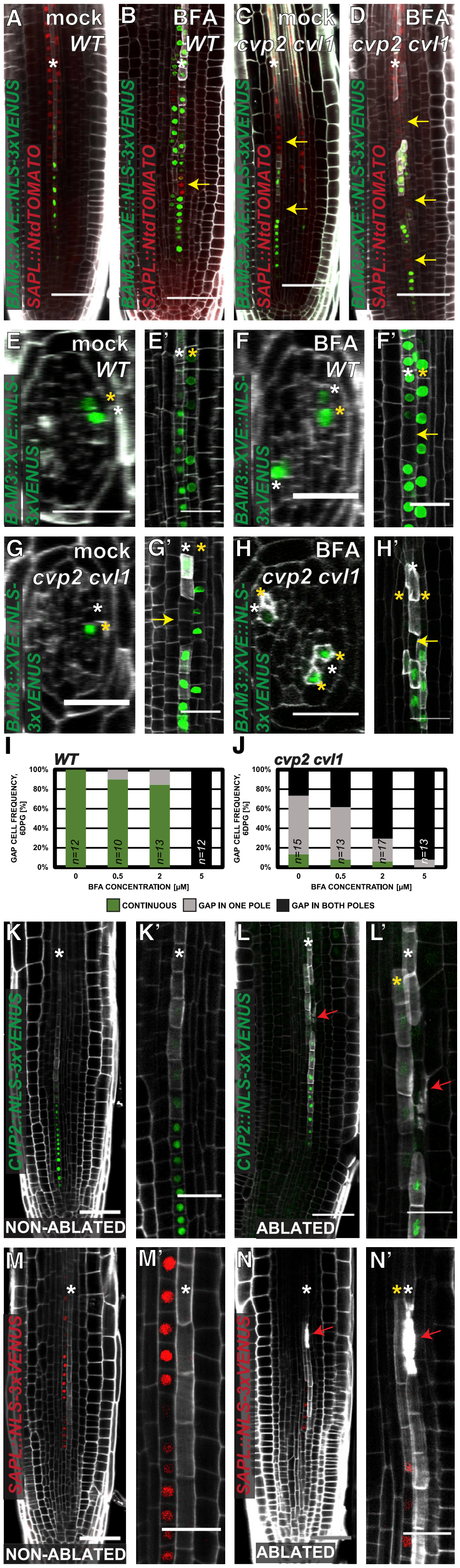

each protophloem strand was ablated by multi-photon laser irradiation and imaged 24 h later. Post-recovery analysis by live imaging revealed the circumvention of the injured protophloem cell by a neighboring one, which was converted into a PSE in 10 out of 15 protophloem strands (Figures 2K–2L'). Similar analysis performed in roots harboring *SAPL::NLS-3×VENUS* confirmed that the cells circumventing the wounded PSE are CCs or MSEs, as they had derived from a *SAPL*-expressing cell file (Figures 2M–2N'). Overall, our results suggest that phloem-primed cells contain a degree of identity plasticity that enables them to reprogram their cell fate (which is originally determined by the cell file to which they belong to) upon positional cues in order to (re) establish a functional phloem pattern. Such plasticity has been observed in proliferating phloem cells, allowing us to predict a spatiotemporal boundary of a phloem "plastic zone." In this zone, proliferating PSE-surrounding cells can temporarily be held in an uncommitted stage until being transferred by newly formed meristematic cells to the region of the root where PSEs start to differentiate. From this point, PSE-surrounding cells (CCs in particular) start expressing their unique set of genes and their lineage will be split from PSE.

RPK2 Excludes PSE Identity from the CC Lineage within the Plastic Zone

To determine the molecular factors underpinning phloem plasticity, we performed a mutagenesis screen to uncover genetic suppressors of the PSE *cvp2 cvl1* hybrid cell identity. Among several mutants isolated, *suppressor of cvp2 cvl1*(*socc*) *9* (*socc9 cvp2 cvl1*) was initially noted for its ability to restore a continuous protophloem strand (Figures 3A–3C' and 3E). As expected, this phenotype is associated with a partial restoration of meristematic activity and post-embryonic root growth (Figures 3F and 3G). To identify the causal mutation responsible for the restored phenotype, *socc9 cvp2 cvl1* plants were backcrossed with *cvp2 cvl1* and their F_2 progeny was analyzed. Long-rooted seedlings ($\leq$25%, as expected for a recessive mutation) were harvested and subjected to next-generation sequencing (NGS) (Figure S2F). This analysis revealed a second-site mutation in the kinase domain of *RECEPTOR PROTEIN LIKE KINASE 2* (*RPK2*/*TOAD2*) [27] as a potential candidate responsible for the rescued phenotype observed in *socc9 cvp2 cvl1* (Figure 3H).

Figure 2. PSE and PSE-Surrounding Identities Are Interchangeable within the Plastic Zone of the Root

(A–D) Confocal microscopy analysis of *BAM3* (4 h induced with 1 µM estradiol) and *SAPL* expression in WT and *cvp2 cvl1* plants treated with 5 µM BFA for 48 h. Note *BAM3* expression at the CC position adjacent to *SAPL*-expressing cells (PSE gap cells) in seedlings treated with BFA.

(E–H') BFA effect on *BAM3* expression in wild-type plants (E–F') and *cvp2 cvl1* (G–H') roots, in which additional PSE-differentiated cells can be observed simultaneously. *BAM3* expression was induced by incubating the seedlings 4 h in 1 µM estradiol. Yellow asterisks mark ectopic *BAM3* expression.

(I and J) Quantification of *cvp2 cvl1* hypersensitivity as manifested by the appearance of gap cells in protophloem strands upon treatments with increasing concentration of BFA.

(K–N') Ectopic protophloem differentiation can be detected in the cells adjacent to the laser-ablated PSE after 24 h of recovery as revealed by cell wall thickening when analyzed by confocal microscopy.

Protophloem strands are marked by white asterisks, yellow asterisks mark PSE neighboring cell file, and red arrows mark PSE ablation site. Scale bars in (A)–(D) and (K)–(N) represent 50 µm; otherwise, 20 µm.

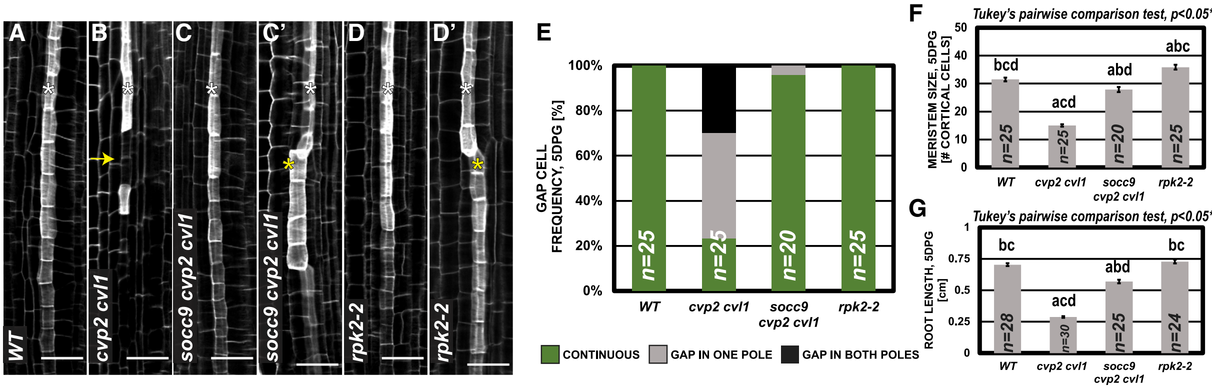

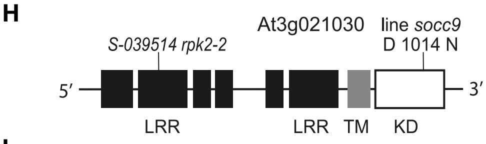

I

Fisher's exact test, two sided, p<0.01**

Genotype	Single File PSE [%]	Shifting PSE [%] Total Shifts	To CCs	To MSE	n
WT [a]	96	4 [bcd]	4	0	100
cvp2 cvl1 [b]	88.2	11.8 [ac]	9.4	2.4	85
socc9 cvp2 cvl1 [c]	80.4	19.6 [abd]	15.2	4.3	92
rpk2-2 [d]	90	10 [ac]	7	3.0	100

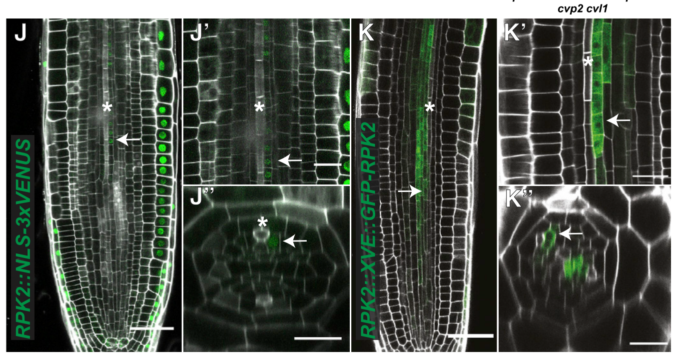

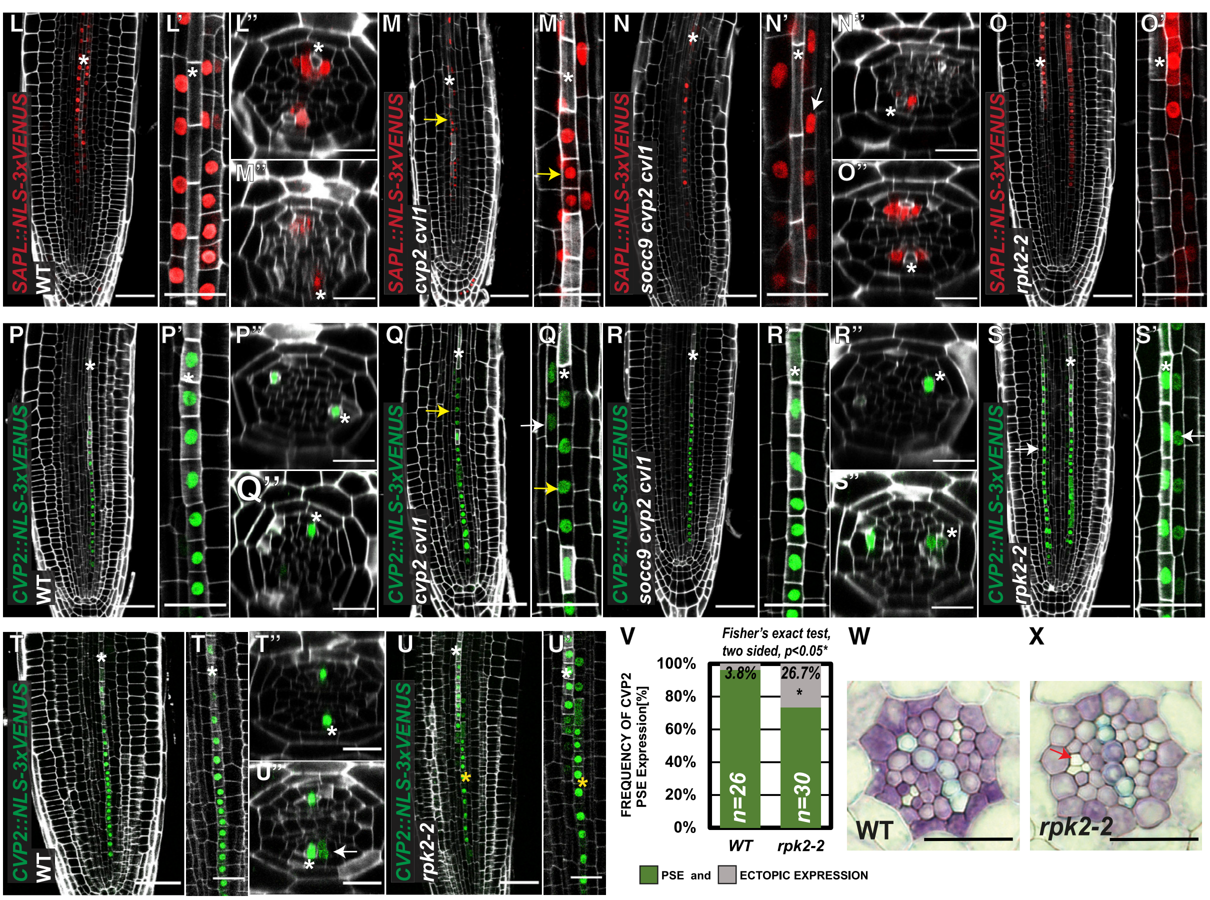

(legend on next page)

As D1014N mutation is located in the kinase domain of RPK2, it may hamper ATP binding and thus render a kinase-dead version of the receptor. Introgression of *RPK2::RPK2-CITRINE* in *socc9 cvp2 cvl1* genetic background restored the short root phenotype of *cvp2 cvl1* in 93.5% of the plants, demonstrating the ability of this construct to complement *socc9* mutation (Figures S2A–S2F). Confirmation of *rpk2* as a suppressor candidate was achieved also by creating an artificial microRNA against *RPK2* (*amiRPK2*), whose efficiency was confirmed by real-time quantitative PCR (qPCR) (Figure S2G). We observed a positive correlation between *RPK2* silencing in *cvp2 cvl1* and the rescue of its protophloem discontinuity (Figures S2G–S2J' and S2L), root meristematic activity (Figure S2M), and root growth (Figure S2N). Similar results were obtained by crossing the null mutant *rpk2*-2 (SALK_039514) with *cvp2 cvl1* (Figures S2O–S2R' and S2W–S2Y). Notably, analogous phenotypes were detected when introducing *rpk2-2* mutation in *ops* and *brx* genetic backgrounds (Figures S2S–S2Y). Closer examination of *socc9 cvp2 cvl1*, *rpk2-2 cvp2 cvl1*, and *amiRPK2 cvp2 cvl1* strands revealed the appearance of two effects when restoring protophloem continuity: a continuous single-stranded PSE cell file (Figures 3C, S2J, and S2R) and a PSE cell file that shifted to a neighboring one (Figures 3C', S2J'–S2K, and S2R'). These observations suggest that, in the shifted PSE position, an identity change must have occurred in the neighboring cell file. Such shifts were also detected in *rpk2-2* single mutants (Figures 3D' and S2P), and although we observed them at low frequency, their appearance tends to increase when introducing *rpk2-2* mutation in *cvp2 cvl1* or *ops* genetic background (24% and 40%, respectively; Figures S2P–S2T' and S2Z). In order to better understand the mechanism of the rescues, we first analyzed *RPK2* expression by confocal microscopy. Besides its predominant expression in the epidermis and lateral root cap, we could also observe an overall weak expression specific to phloem pole pericycle and CCs (Figures 3J–3J''). To visualize the weaker vascular expression of *RPK2*, we generated an estradiol-inducible RPK2 protein tagged with GFP at the N terminus (*RPK2::XVE::GFP-RPK2*). Confocal microscopy analysis of roots incubated in 2 μM estradiol (ES) for 5 h demonstrated RPK2 accumulation in PSE-surrounding cells and occasionally in the procambium (Figures 3K–3K''). Notably, RPK2 accumulation within the phloem coincided with the region where PSE cells exit the proliferative phase and begin to differentiate. We thus sought to determine how *rpk2* mutation could restore a normal phloem identity in *cvp2 cvl1* by examining *SAPL* expression in *socc9 cvp2 cvl1* roots. Contrary to *cvp2 cvl1*, where *SAPL* expression could be detected within PSEs, this gene was restricted to the PSE-surrounding cells in *socc9 cvp2 cvl1* (Figures 3L–3O''). As expected, *socc9 cvp2 cvl1* displays a continuous *CVP2* expression within the protophloem strand (Figures 3P–3R''), prompting us to assess how *rpk2* mutation alone could affect protophloem and CC identities. Examination of the protophloem-specific *CVP2* marker in *rpk2-2* roots revealed the ectopic expression of this gene in PSE-surrounding cells (27% frequency versus 4% frequency in wild-type; Figures 3S–3V). Furthermore, the lateral expansion of PSE identity observed in *rpk2* occurring toward the neighboring MSE (Figures 3S–3S'') or CC (Figures 3T–3U'') can translate into the coexistence of an additional PSE next to the original PSE cell file for a short stretch of cells (Figures 3W and 3X). This implies that RPK2 partially functions in restricting PSE identity, among proliferating phloem cells, to the PSE position. However, the low number of shifts observed in the *rpk2* single mutant (10%; Figure 3I) suggests that other players may counteract this phenomenon. Yet the potential to expand the PSE domain may be utilized when combined with other genetic backgrounds, such as *cvp2 cvl1* or *ops-2*, when frequency of PSE shifts can increase substantially to 20%–24% and 40%, respectively (Figures S2Z and 3I). To further explore the spatiotemporal requirement of RPK2 activity, we decided to silence *RPK2* expression under distinct phloem promoters in a *cvp2 cvl1* genetic background. *amiRPK2* expression under *NaKR1* promoter, normally active after the root transition zone in CCs, did not rescue the *cvp2 cvl1* hybrid identity within gap cells (Figures S3A–S3C and S3F). Interestingly, silencing *RPK2* in *BAM3*-expressing cells resulted in the partial restoration of all *cvp2 cvl1* root phenotypes and coincided with the highest frequency of PSE shifts (Figures S3A–S3D and S3F–S3I). Because *BAM3* is occasionally expressed at the CC position within the plastic zone (Figures 2E, 2E', 2G, and 2G'), it is likely that the rescue of *cvp2 cvl1* by *BAM3::amiRPK2* is due to *RPK2* silencing also in these cells. Furthermore, our results imply that PSE shifting to a neighboring cell file can be utilized as an additional mechanism to ensure protophloem continuity. In contrast, the partial rescue displayed by *CVP2::amiRPK2* could be explained by the downregulation of

Figure 3. RPK2 Suppresses Lateral Expansion of Protophloem Identity, and Its Deficiency Rescues *cvp2 cvl1*

(A–D') Confocal microscopy images of the root protophloem strands of the indicated genotypes. 6-day-old plants were fixed and stained with Calcofluor White.

(E) Quantification of gap appearance in *suppressor of cvp2 cvl1 9* (*socc9 cvp2 cvl1*), *cvp2 cvl1*, *rpk2-2*, and WT protophloem strands.

(F and G) Restoration of meristematic activity (F) and root growth (G) in *socc9 cvp2 cvl1*. Bars indicate the SE. Different letters indicate significant differences among indicated genotypes.

(H) Schematic representation of *RPK2* gene structure showing the domains affected by the isolated mutation found in *socc9* and the transfer DNA (T-DNA) insertion in *rpk2*-2.

(I) Quantification of shift appearance in protophloem strands.

(J–J'') *RPK2* expression pattern within the root and the meristematic stele.

(K–K'') Protein distribution of *RPK2* within the root meristem as revealed by the analysis of *RPK2::XVE::GFP-RPK2* seedlings incubated in estradiol for 5 h and stained with propidium iodide for microscopy imaging.

(L–O'') Analysis of *SAPL* expression in the indicated genotypes.

(P–U'') Confocal images of *CVP2::NLS-3×VENUS* in WT, *cvp2 cvl1*, *socc9 cvp2 cvl1*, and *rpk2-2*. In *rpk2*-2, an expanded lateral protophloem domain can be observed based on *CVP2* expression analysis. Images of control roots for (U–U'') are displayed in (T–T''), as were part of an independent experiment.

(V) Quantification of ectopic *CVP2* expression in *rpk2-2* versus WT.

(W and X) Toluidine-blue-stained orthogonal sections of WT and *rpk2-2* roots, showing an additional PSE at the CC position in *rpk2-2* (red arrow).

PSE strands are marked by white asterisks, and yellow asterisks label PSE-surrounding cells. Yellow arrows indicate gap cells, and white arrows indicate relevant gene expression or protein localization. Scale bars in (J)–(U) represent 50 μm; otherwise, 20 μm. See also Figures S2 and S3.

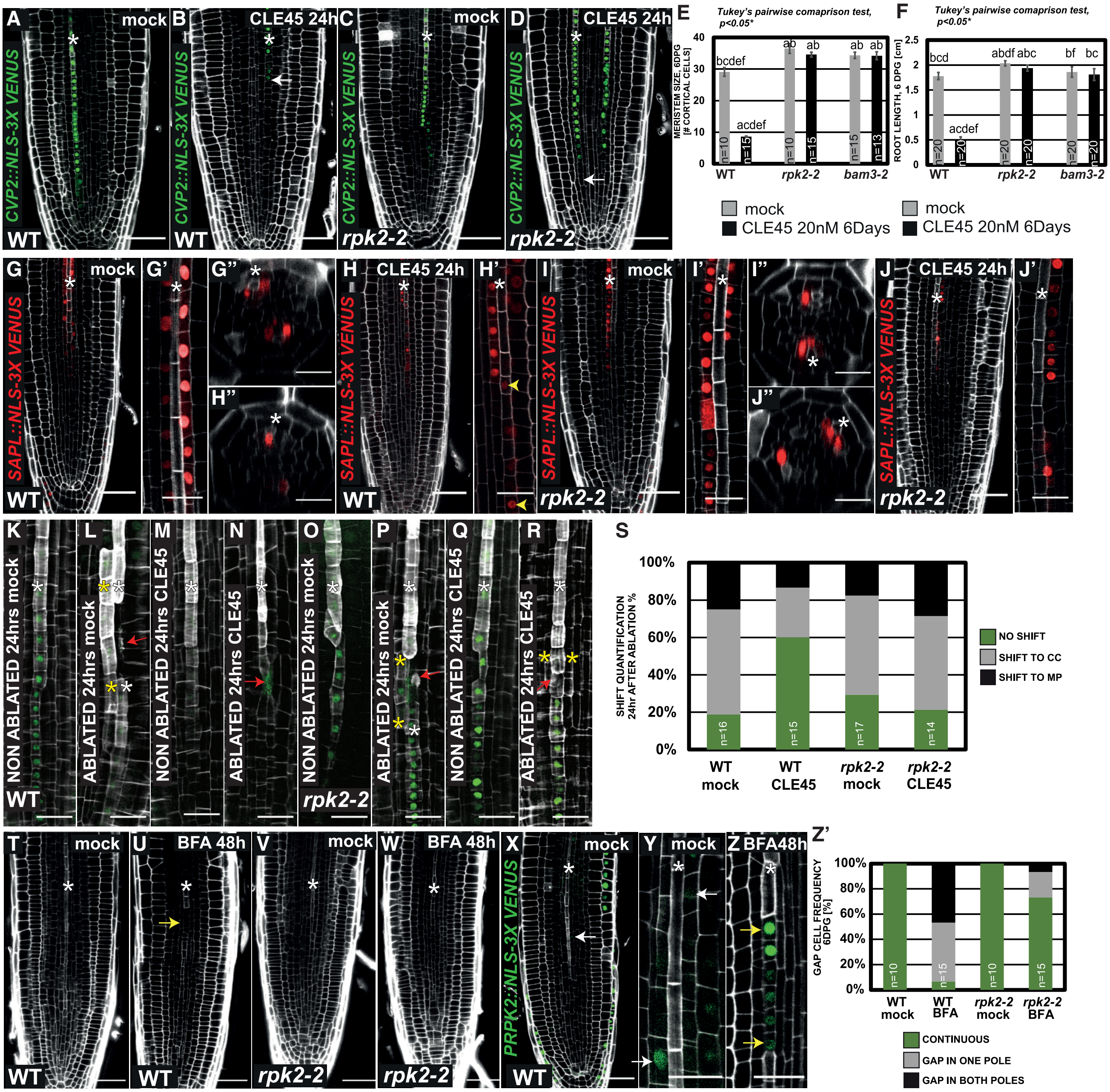

Figure 4. CLE45 Perception by RPK2 Contributes to Confer Plasticity to Phloem Cells by Re-setting Their Identity to a Pluripotent Stage

(A–D) *rpk2-2* resistance to CLE45-mediated suppression of protophloem formation as revealed by analysis of *CVP2* expression.

(E and F) Quantification of meristematic activity and root length of the indicated genotypes grown in media supplemented with 20 nM CLE45. *bam3* mutant is used as a negative control. Bars indicate the SE. Different letters indicate significant differences among indicated genotypes.

(G–J'') Analysis of *SAPL* expression in phloem cells of 20 nM CLE45-treated plants for 24 h. *rpk2-2* is resistant to the identity switch of PSE, triggered by CLE45 signaling (I–J'').

(K–R) CLE45 partially prevents formation of new PSE cells in roots in which proliferating PSEs were ablated. Confocal microscopy analysis of WT and *rpk2-2* seedlings harboring *CVP2::NLS3-×VENUS* exposed for 24 h to 20 nM CLE45 after ablation experiments is shown. Ablated cells are marked by red arrows, and newly formed PSE cells are marked by yellow asterisks.

(S) Quantification of shifts appearance in roots displayed in (K)–(R) upon CLE45 treatments.

(T–W) *rpk2-2* is partially resistant to the BFA-mediated gap appearance, as revealed by confocal microscopy examination of their protophloem strands after 48 h treatment.

(X–Z) *RPK2* expression in gap cells of plants incubated in 5 μM BFA for 48 h as revealed by confocal microscopy analysis of *RPK2::NLS-3×VENUS*.

(legend continued on next page)

RPK2 within gap cells, enforcing PSE cell fate and committing them to this developmental trajectory (Figures S3E–S3I).

RPK2 Conveys CLE45 Signal to Confer Cell Plasticity within the Phloem

We next sought to elucidate how RPK2 may exclude PSE identity from the PSE-surrounding cells. This LRR-like receptor was involved in the perception of several CLE peptides to modulate different aspects of root development [28, 29]. Although *rpk2-2* is resistant to many tested CLE peptides in suppressing the post-embryonic growth of the root (Figure S4A), we decided to focus on its role in perceiving the ones previously described to affect phloem tissues, such as CLE25, CLE26, and CLE45 [4, 9, 30] (Figures S4B–S4B''). Consistent with previous observations, *CVP2* expression is severely delayed upon CLE25, CLE26, and CLE45 treatments, but not upon phloem-unrelated CLE41/44 treatment (Figures 4A, 4B, and S4C–S4G') [4, 10]. Surprisingly, 24 h of CLE45 treatment delayed *SAPL::NLS-3×VENUS* in PSE-surrounding cells but also altered its expression domain moving it into the protophloem strand (Figures 4G–4H'', S4K, and S4K'). Similar results were obtained when subjecting wild-type seedlings to CLE25 and CLE26 treatments (Figures S4H–S4L'). However, to attain an in-depth understanding of how phloem identity is regulated, we decided to focus our efforts mainly on one, CLE45, as it has been previously described that it suppresses the transition between proliferation and differentiation of PSE cells in an autocrine fashion [4]. Contrary to wild-type roots, *CVP2* expression remains unaffected in *rpk2-2* roots treated with CLE45, demonstrating the capacity of RPK2 in conveying CLE45 signal (Figures 4A–4F). The ectopic CLE45-mediated *SAPL* expression in PSE was not observed in *rpk2-2* protophloem strands (Figures 4G–4J''). These results highlight the contribution of CLE45 perception in *RPK2*-expressing cells to regulate PSE identity. Although affecting *CVP2* expression, CLE45 treatment did not alter the expression of genes acting in earlier phloem developmental stages, such as *AUX1* or *SMXL3* (Figures S4M–S4N') [31, 32], excluding CLE45 activity from the development of phloem stem cells. Based on *CLE45* expression pattern and these observations (Figures S4B–S4B''), it can be speculated that phloem plasticity occurs when cells undergo proliferation, but the PSE cell file has not yet been committed to its cell lineage. Thus, it appears that the boundaries of PSE identity must be established at this developmental stage, before PSE and MSE identities are separated, otherwise resulting in cell identity hybridism. Because CLE45 peptide cannot be tagged by a fluorescent protein as it undergoes posttranslational modifications [33], at this stage, we cannot determine its exact distribution within the phloem tissues. Yet it appears possible that CLE45 is radially distributed from the PSE to the surrounding elements. To further determine the role of CLE45 in regulating the PSE-surrounding cells development, we analyzed their capacity to take on PSE identity and differentiate after PSE ablation and recovery for 24 h on CLE45-supplemented media. Quantification of newly formed PSE cells at CC or MSE position adjacent to the ablation site in CLE45 recovered roots revealed a reduced number of shifts in comparison to recovery in mock conditions (Figures 4K–4S). These findings suggest that a CLE45 field can also suppress the ability of PSE-surrounding cells to become PSEs, however, supporting our results that these cells can sense CLE45. Remarkably, CLE45 did not affect recovery of ablated PSE strands in *rpk2-2* background (Figures 4O–4S), supporting the notion that RPK2 is involved in CLE45-mediated prevention of PSE-surrounding cells fate commitment. However, at this point, we cannot exclude the fact that, in addition to keeping the phloem cells uncommitted (to PSE or CC lineage), CLE45 also prevents PSE differentiation, as reported before [9]. To further explore RPK2 involvement in this process, we decided to examine *rpk2-2* sensitivity to the gap-induced effect of BFA. The lower frequency of gap cells observed in *rpk2*-2 roots incubated in a medium supplemented with BFA for 48 h confirms that RPK2 function is part of the mechanism by which this drug triggers the appearance of gap cells (Figures 4T–4W and 4Z'). Moreover, *RPK2* expression was detected in BFA-triggered gap cells (Figures 4X–4Z), suggesting that *RPK2* transcripts are part of the hybrid identity observed in these cells. Collectively, our data suggest that RPK2 activity in perceiving CLE45 and/or other similar CLE peptides contributes to maintain a plastic zone within the root phloem (Figure 5). By modulating CLE perception at the single-cell level, plant cells can re-pattern a functional phloem pole by maintaining a reservoir of uncommitted phloem cells endowed with the ability to switch their cell fate upon positional cues.

DISCUSSION

The Developmental Plasticity of Phloem Cells to Re-pattern a Functional Phloem Pole

Contrary to animal cells, in which cell identity is mainly lineage determined, plant cells exhibit the ability to reprogram their cell identity based on positional cues. Yet a fundamental question in plant development is how cell pluripotency lies at the core of the developmental program of the cells already committed to a particular cell fate. Classical studies have already highlighted the plasticity of plant cells in de-differentiating and reprograming their cell identities *in vitro* [2]. However, examples of the importance of cell plasticity *in vivo* have only recently begun to emerge. Such examples include the mechanisms restoring excised root tips by recapitulating an embryonic pattern or the underlying mechanisms replacing injured cells [1, 34]. Yet very little is known about the post-embryonic circuits involved in the maintenance of pluripotent non-stem cells. In this work, we show how the identity of PSE-surrounding cells can remain uncommitted until PSE differentiation occurs, generating a short spatiotemporal window in which phloem cells can re-pattern a phloem pole in case of disruption of the protophloem strand (Figures 2K–2N'). CCs are known for their importance in supporting the differentiated PSEs and for being the entry route, to conductive phloem tissues, for viruses

(Z') Quantification of the number of gap cells found in the protophloem strands of BFA-treated plants.

White asterisks mark protophloem strands, yellow arrows indicate gap cells, and yellow arrowheads mark *SAPL* expression in the protophloem strand. White arrows indicate where expression onset occurs, and yellow asterisks mark ectopic PSE formation. Scale bars in (A)–(D), (G)–(J), and (T)–(X) represent 50 μm; otherwise, 20 μm. See also Figure S4.

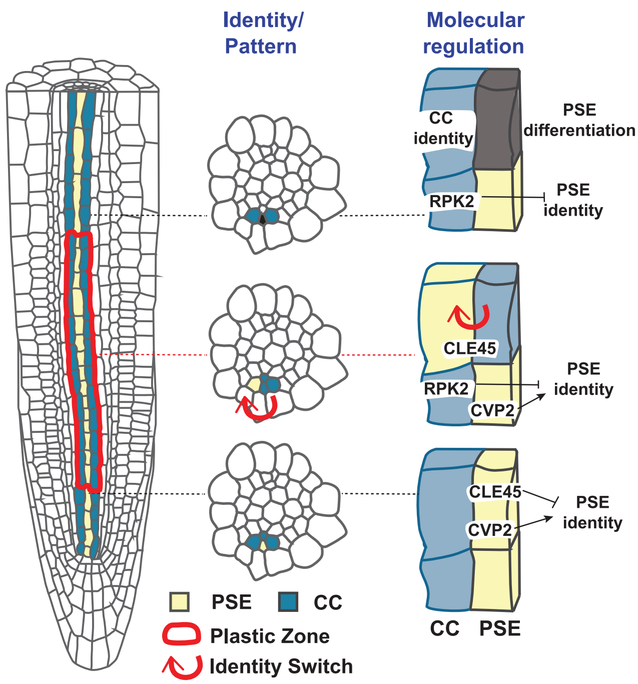

Figure 5. Schematic Overview of the Molecular Mechanisms Regulating PSE Identity and Phloem Patterning in *Arabidopsis* Roots

A longitudinal view (left) and radial view (middle) of the developmental trajectories of protophloem sieve elements (PSEs) and companion cells (CCs) within the root are represented. Previous to their entry into the plastic zone (surrounded in red), future PSE cells acquire their cell identity and enter into a proliferative phase, a process partially regulated by the activity of positive regulators (such as CVP2) and counteracted by negative regulators, such as CLE peptides. Within the plastic zone, PSE-surrounding elements are primed as phloem cells, but they still exhibit plastic identity and can switch their identity (red arrows) according to positional cues. Once PSE cells enter into differentiation process, RPK2 excludes PSE identity from PSE-surrounding cells, allowing these cells to commit to CC's developmental trajectory.

and growth regulators, such as FLORIGEN [35]. Although these functions clearly highlight a role for CCs upon PSE differentiation, our work reveals their importance at earlier developmental stages. Indeed, proliferating CCs and MSEs constitute a reservoir of phloem cells with plastic development that can switch their identity triggered by PSE misspecification in order to ensure the correct formation of a conductive strand (Figure 5). However, in mutants with interrupted development of PSE strands, this plasticity cannot be used, as reflected by the appearance of gap cells. Gap cells in *cvp2 cvl1*, *brx*, or *ops* mutants have been interpreted as undifferentiated protophloem cells [4, 6, 12, 36]; however, our observations point out that gap cells are a consequence of PSE misspecification in earlier stages. In particular, the emergence of gap cells is tightly coupled with the identity hybridism and partial commitment of a PSE-positioned cell to a CC cell fate as suggested by the expression of mature CC-associated transporters, such as *NaKR1* (Figures 1L–1M'). Interestingly, in these mutants, PSE cannot be formed in adjacent cells, and thus, the PSE file stays disconnected, pointing toward the existence of a mechanism preventing the formation of a PSE outside of its position. Why does the existing plasticity, observed in phloem cells, never translate into the coexistence of several PSE files? In particular, the PSE is always five-angled in a traverse section, with one of the angles inserted in between two pericycle cell files, a feature highly conserved in a wide variety of dicotyledons plants [37]. Owing to the presence of highly specialized plasmodesmata connecting sieve element and the PPP [7], it appears plausible that the formation of several PSEs per phloem pole is repressed to preserve the correct functionality of sieve element-PPP connection in regulating the phloem unloading in discrete pulses to the root meristem. Accordingly, phloem plasticity is only retained until protophloem cells enter into their differentiation program, consistent with the recent notion of a gradual progression from stemness to differentiation within the whole root meristem [38]. Nevertheless, similar mechanisms involving procambial cells may exist in the mature part of the root to ensure the correct formation of metaphloem conductive tissues, but this hypothesis awaits further investigation. The presence of plastic phloem cells could confer an advantage to plants as a healing mechanism. In grafted plants, the first vascular tissue to establish a continuous network in the stem is the phloem [39]. Although we lack a description of this process at single-cell-level resolution, it seems likely that the presence of a pool of pluripotent phloem-primed cells could greatly contribute to re-establishing a functional tissue.

CLE45-RPK2 Module Contributes to Maintain Phloem Plasticity

The underlying signaling cascades of phloem plasticity remain poorly understood. Yet we provide insights on how the putative module CLE45-RPK2 contributes to this process. The prevention of PSE-surrounding cells to differentiate as PSE, recovered after the ablation of proliferating PSE cells on CLE45-supplemented media (Figures 4K–4N), indicates the importance of CLE45 perception in cell files outside of its expression domain. Moreover, it indicates that a clearance of the local CLE45 signaling must occur in order for the neighboring uncommitted cell to differentiate as a PSE. Surprisingly, neither mature gap cells of *cvp2 cvl1* nor BFA-triggered PSE gaps exhibited *CLE45* expression (Figures S4O–S4Q'). The loss of local CLE45 signaling should, in turn, commit the cell adjacent to the gap cell to a PSE lineage. However, this does not occur in *cvp2 cvl1*, where CC identity is acquired at the PSE position (Figures 1L–1O) and the re-establishment of a new PSE fails. The resistance of *rpk2-2* to other CLE peptides, such as CLE25 or CLE26, suggests that the coordinated activity of several CLE peptides and receptors is required to confer plasticity to phloem cells (Figures S4A and S4C–S4E'). For instance, it is possible that RPK2 participates in the signaling of root-active CLE peptides in combination with other well-known phloem regulators, such as BAM3 or CLERK [10, 30]. The partial or total suppression of protophloem defects when introducing *rpk2-2* mutation in *ops* or *brx* further supports this notion (Figures S2O–S2W). Recent studies have indicated that OPS attenuates CLE45 action by interfering with components of its signaling cascade [40]. An enhanced CLE45 signaling in the meristematic PSEs and CCs could increase the plastic identity of these cells, a hypothesis consistent with the appearance of the highest number of shifts observed in *rpk2-2 ops* in comparison to the other gap-containing mutants (Figure S2Z). Although *CLE45* is specifically expressed in the protophloem strand within the root meristem, its expression switches to the PSE-surrounding cells after PSE enucleation

(Figures S4B–S4B''). This may imply that CLE45 acts in a cell-autonomous manner to coordinate the future formation of MSE in the mature part of the root. Alternatively, the effect of CLE45 on suppressing phloem identity is the result of its synergistic perception at the single-cell level by distinct receptors (i.e., BAM3-RPK2 and CORYNE-CLAVATA-RPK2). Indeed, CORYNE has been recently described to stabilize BAM3 distribution within the stele [10]. Because RPK2 can interact with BAM1 to regulate cell proliferation within the root meristem [29], it appears possible that the root may establish a gradient of CLE45 signaling by modulating the dynamics of its receptors. To this end, previous studies have shown the role of *CVP2* and *CVL1* in modulating vesicle trafficking in protophloem cells [12]. An enrichment of the CVP2- and CVL1-enzymatic product PtdIns(4,5)P_2 at the plasma membrane redirects vesicle trafficking toward the vacuole [12] and may potentially displace plasma-membrane-localized receptors essential for proper CLE peptide signaling. However, further investigation is necessary in order to decipher the complex molecular mechanisms underlying the formation of a functional phloem pole.

STAR★METHODS

Detailed methods are provided in the online version of this paper and include the following:

- KEY RESOURCES TABLE
- LEAD CONTACT AND MATERIALS AVAILABILITY
- EXPERIMENTAL MODEL AND SUBJECT DETAILS
- METHOD DETAILS
  - Plant material and growth conditions
  - Cloning and plant transformation
  - Microscopic analysis and histology
  - SBFSEM
  - FACS, RNA isolation and RNA library preparation
  - RNA isolation and quantitative RT-PCR
  - EMS mutagenesis, DNA extraction, library preparation and Next Generation Sequencing
- QUANTIFICATION AND STATISTICAL ANALYSIS
- DATA AND CODE AVAILABILITY

SUPPLEMENTAL INFORMATION

Supplemental Information can be found online at https://doi.org/10.1016/j.cub.2019.12.043.

ACKNOWLEDGMENTS

We greatly thank Dr. Ross Sozzani and Adam Fischer for their critical assistance in RNA sequencing experiments, Dr. Sam Zeeman for his help with SBFSEM, Dr. Thomas Greb and Dr. Christian Hardtke for kindly providing seeds, Functional Genomic Center of Zurich and ScopeM for their services, and E. Robinson for technical support. B.G. and E.K. were funded by Vontobel and Stravros Niarchos Foundations, respectively. M.A.R.-S. was funded by ETH (ETH-33 12-1). This work was funded by the Swiss National Foundation (SNF_31003A_160201 to A.R.-V.).

AUTHOR CONTRIBUTIONS

B.G., E.K., and A.R.-V. designed the research. B.G., E.K., A.S., M.A.R.-S., S.E., and T.M.D.C. performed the experiments. E.T., R.D., B.G., E.K., and T.M.D.C. analyzed the data. A.R.-V., E.K., and B.G. wrote the manuscript.

DECLARATION OF INTERESTS

The authors declare no competing interests.

Received: August 30, 2019
Revised: November 15, 2019
Accepted: December 12, 2019
Published: February 6, 2020

REFERENCES

1. Efroni, I., Mello, A., Nawy, T., Ip, P.L., Rahni, R., DelRose, N., Powers, A., Satija, R., and Birnbaum, K.D. (2016). Root regeneration triggers an embryo-like sequence guided by hormonal interactions. Cell *165*, 1721–1733.
2. Skoog, F., and Miller, C.O. (1957). Chemical regulation of growth and organ formation in plant tissues cultured in vitro. Symp. Soc. Exp. Biol. *11*, 118–130.
3. Lucas, W.J., Groover, A., Lichtenberger, R., Furuta, K., Yadav, S.R., Helariutta, Y., He, X.Q., Fukuda, H., Kang, J., Brady, S.M., et al. (2013). The plant vascular system: evolution, development and functions. J. Integr. Plant Biol. *55*, 294–388.
4. Rodriguez-Villalon, A., Gujas, B., Kang, Y.H., Breda, A.S., Cattaneo, P., Depuydt, S., and Hardtke, C.S. (2014). Molecular genetic framework for protophloem formation. Proc. Natl. Acad. Sci. USA *111*, 11551–11556.
5. Miyashima, S., Roszak, P., Sevilem, I., Toyokura, K., Blob, B., Heo, J.O., Mellor, N., Help-Rinta-Rahko, H., Otero, S., Smet, W., et al. (2019). Mobile PEAR transcription factors integrate positional cues to prime cambial growth. Nature *565*, 490–494.
6. Truernit, E., Bauby, H., Belcram, K., Barthélémy, J., and Palauqui, J.C. (2012). OCTOPUS, a polarly localised membrane-associated protein, regulates phloem differentiation entry in Arabidopsis thaliana. Development *139*, 1306–1315.
7. Ross-Elliott, T.J., Jensen, K.H., Haaning, K.S., Wager, B.M., Knoblauch, J., Howell, A.H., Mullendore, D.L., Monteith, A.G., Paultre, D., Yan, D., et al. (2017). Phloem unloading in Arabidopsis roots is convective and regulated by the phloem-pole pericycle. eLife *6*, e24125.
8. Furuta, K.M., Yadav, S.R., Lehesranta, S., Belevich, I., Miyashima, S., Heo, J.O., Vatén, A., Lindgren, O., De Rybel, B., Van Isterdael, G., et al. (2014). Plant development. Arabidopsis NAC45/86 direct sieve element morphogenesis culminating in enucleation. Science *345*, 933–937.
9. Depuydt, S., Rodriguez-Villalon, A., Santuari, L., Wyser-Rmili, C., Ragni, L., and Hardtke, C.S. (2013). Suppression of Arabidopsis protophloem differentiation and root meristem growth by CLE45 requires the receptor-like kinase BAM3. Proc. Natl. Acad. Sci. USA *110*, 7074–7079.
10. Hazak, O., Brandt, B., Cattaneo, P., Santiago, J., Rodriguez-Villalon, A., Hothorn, M., and Hardtke, C.S. (2017). Perception of root-active CLE peptides requires CORYNE function in the phloem vasculature. EMBO Rep. *18*, 1367–1381.
11. Rodriguez-Villalon, A., Gujas, B., van Wijk, R., Munnik, T., and Hardtke, C.S. (2015). Primary root protophloem differentiation requires balanced phosphatidylinositol-4,5-biphosphate levels and systemically affects root branching. Development *142*, 1437–1446.
12. Gujas, B., Cruz, T.M.D., Kastanaki, E., Vermeer, J.E.M., Munnik, T., and Rodriguez-Villalon, A. (2017). Perturbing phosphoinositide homeostasis oppositely affects vascular differentiation in *Arabidopsis thaliana* roots. Development *144*, 3578–3589.
13. Ruiz Sola, M.A., Coiro, M., Crivelli, S., Zeeman, S.C., Schmidt Kjølner Hansen, S., and Truernit, E. (2017). OCTOPUS-LIKE 2, a novel player in Arabidopsis root and vascular development, reveals a key role for OCTOPUS family genes in root metaphloem sieve tube differentiation. New Phytol. *216*, 1191–1204.
14. Anstead, J.A., Froelich, D.R., Knoblauch, M., and Thompson, G.A. (2012). Arabidopsis P-protein filament formation requires both AtSEOR1 and AtSEOR2. Plant Cell Physiol. *53*, 1033–1042.

15. Chen, L.Q., Qu, X.Q., Hou, B.H., Sosso, D., Osorio, S., Fernie, A.R., and Frommer, W.B. (2012). Sucrose efflux mediated by SWEET proteins as a key step for phloem transport. Science *335*, 207–211.

16. Batailler, B., Lemaître, T., Vilaine, F., Sanchez, C., Renard, D., Cayla, T., Beneteau, J., and Dinant, S. (2012). Soluble and filamentous proteins in Arabidopsis sieve elements. Plant Cell Environ. *35*, 1258–1273.

17. Cayla, T., Batailler, B., Le Hir, R., Revers, F., Anstead, J.A., Thompson, G.A., Grandjean, O., and Dinant, S. (2015). Live imaging of companion cells and sieve elements in Arabidopsis leaves. PLoS ONE *10*, e0118122.

18. Brady, S.M., Orlando, D.A., Lee, J.Y., Wang, J.Y., Koch, J., Dinneny, J.R., Mace, D., Ohler, U., and Benfey, P.N. (2007). A high-resolution root spatiotemporal map reveals dominant expression patterns. Science *318*, 801–806.

19. Vilaine, F., Kerchev, P., Clément, G., Batailler, B., Cayla, T., Bill, L., Gissot, L., and Dinant, S. (2013). Increased expression of a phloem membrane protein encoded by NHL26 alters phloem export and sugar partitioning in Arabidopsis. Plant Cell *25*, 1689–1708.

20. Hirayama, T., Lei, G.J., Yamaji, N., Nakagawa, N., and Ma, J.F. (2018). The putative peptide gene FEP1 regulates iron deficiency response in Arabidopsis. Plant Cell Physiol. Published online July 19, 2018. 10.1093/pcp/pcy145.

21. Mao, J.L., Miao, Z.Q., Wang, Z., Yu, L.H., Cai, X.T., and Xiang, C.B. (2016). Arabidopsis ERF1 mediates cross-talk between ethylene and auxin biosynthesis during primary root elongation by regulating ASA1 expression. PLoS Genet. *12*, e1005760.

22. Kanno, Y., Oikawa, T., Chiba, Y., Ishimaru, Y., Shimizu, T., Sano, N., Koshiba, T., Kamiya, Y., Ueda, M., and Seo, M. (2016). AtSWEET13 and AtSWEET14 regulate gibberellin-mediated physiological processes. Nat. Commun. *7*, 13245.

23. Nakayama, T., Shinohara, H., Tanaka, M., Baba, K., Ogawa-Ohnishi, M., and Matsubayashi, Y. (2017). A peptide hormone required for Casparian strip diffusion barrier formation in Arabidopsis roots. Science *355*, 284–286.

24. Tian, H., Baxter, I.R., Lahner, B., Reinders, A., Salt, D.E., and Ward, J.M. (2010). Arabidopsis NPCC6/NaKR1 is a phloem mobile metal binding protein necessary for phloem function and root meristem maintenance. Plant Cell *22*, 3963–3979.

25. Geldner, N., Anders, N., Wolters, H., Keicher, J., Kornberger, W., Muller, P., Delbarre, A., Ueda, T., Nakano, A., and Jürgens, G. (2003). The Arabidopsis GNOM ARF-GEF mediates endosomal recycling, auxin transport, and auxin-dependent plant growth. Cell *112*, 219–230.

26. Marhava, P., Bassukas, A.E.L., Zourelidou, M., Kolb, M., Moret, B., Fastner, A., Schulze, W.X., Cattaneo, P., Hammes, U.Z., Schwechheimer, C., and Hardtke, C.S. (2018). A molecular rheostat adjusts auxin flux to promote root protophloem differentiation. Nature *558*, 297–300.

27. Nodine, M.D., Yadegari, R., and Tax, F.E. (2007). RPK1 and TOAD2 are two receptor-like kinases redundantly required for arabidopsis embryonic pattern formation. Dev. Cell *12*, 943–956.

28. Racolta, A., Nodine, M.D., Davies, K., Lee, C., Rowe, S., Velazco, Y., Wellington, R., and Tax, F.E. (2018). A common pathway of root growth control and response to CLE peptides through two receptor kinases in *Arabidopsis*. Genetics *208*, 687–704.

29. Shimizu, N., Ishida, T., Yamada, M., Shigenobu, S., Tabata, R., Kinoshita, A., Yamaguchi, K., Hasebe, M., Mitsumasu, K., and Sawa, S. (2015). BAM 1 and RECEPTOR-LIKE PROTEIN KINASE 2 constitute a signaling pathway and modulate CLE peptide-triggered growth inhibition in Arabidopsis root. New Phytol. *208*, 1104–1113.

30. Anne, P., Amiguet-Vercher, A., Brandt, B., Kalmbach, L., Geldner, N., Hothorn, M., and Hardtke, C.S. (2018). CLERK is a novel receptor kinase required for sensing of root-active CLE peptides in *Arabidopsis*. Development *145*, dev162354.

31. Wallner, E.S., López-Salmerón, V., Belevich, I., Poschet, G., Jung, I., Grünwald, K., Sevilem, I., Jokitalo, E., Hell, R., Helariutta, Y., et al. (2017). Strigolactone- and karrikin-independent SMXL proteins are central regulators of phloem formation. Curr. Biol. *27*, 1241–1247.

32. Swarup, R., Kargul, J., Marchant, A., Zadik, D., Rahman, A., Mills, R., Yemm, A., May, S., Williams, L., Millner, P., et al. (2004). Structure-function analysis of the presumptive Arabidopsis auxin permease AUX1. Plant Cell *16*, 3069–3083.

33. Murphy, E., Smith, S., and De Smet, I. (2012). Small signaling peptides in Arabidopsis development: how cells communicate over a short distance. Plant Cell *24*, 3198–3217.

34. Marhavý, P., Montesinos, J.C., Abuzeineh, A., Van Damme, D., Vermeer, J.E., Duclercq, J., Rakusová, H., Nováková, P., Friml, J., Geldner, N., and Benková, E. (2016). Targeted cell elimination reveals an auxin-guided biphasic mode of lateral root initiation. Genes Dev. *30*, 471–483.

35. Otero, S., and Helariutta, Y. (2017). Companion cells: a diamond in the rough. J. Exp. Bot. *68*, 71–78.

36. Scacchi, E., Salinas, P., Gujas, B., Santuari, L., Krogan, N., Ragni, L., Berleth, T., and Hardtke, C.S. (2010). Spatio-temporal sequence of cross-regulatory events in root meristem growth. Proc. Natl. Acad. Sci. USA *107*, 22734–22739.

37. Essau, K. (1969). The Phloem. Encyclopedia of Plant Anatomy (Gebrueder Borntraeger).

38. Wendrich, J.R., Möller, B.K., Li, S., Saiga, S., Sozzani, R., Benfey, P.N., De Rybel, B., and Weijers, D. (2017). Framework for gradual progression of cell ontogeny in the *Arabidopsis* root meristem. Proc. Natl. Acad. Sci. USA *114*, E8922–E8929.

39. Melnyk, C.W., Schuster, C., Leyser, O., and Meyerowitz, E.M. (2015). A developmental framework for graft formation and vascular reconnection in Arabidopsis thaliana. Curr. Biol. *25*, 1306–1318.

40. Breda, A.S., Hazak, O., Schultz, P., Anne, P., Graeff, M., Simon, R., and Hardtke, C.S. (2019). A cellular insulator against CLE45 peptide signaling. Curr. Biol. *29*, 2501–2508.e3.

41. Carland, F., and Nelson, T. (2009). CVP2- and CVL1-mediated phosphoinositide signaling as a regulator of the ARF GAP SFC/VAN3 in establishment of foliar vein patterns. Plant J. *59*, 895–907.

42. Rodrigues, A., Santiago, J., Rubio, S., Saez, A., Osmont, K.S., Gadea, J., Hardtke, C.S., and Rodriguez, P.L. (2009). The short-rooted phenotype of the brevis radix mutant partly reflects root abscisic acid hypersensitivity. Plant Physiol. *149*, 1917–1928.

43. Trapnell, C., Hendrickson, D.G., Sauvageau, M., Goff, L., Rinn, J.L., and Pachter, L. (2013). Differential analysis of gene regulation at transcript resolution with RNA-seq. Nat. Biotechnol. *31*, 46–53.

44. Clark, N.M., Buckner, E., Fisher, A.P., Nelson, E.C., Nguyen, T.T., Simmons, A.R., de Luis Balaguer, M.A., Butler-Smith, T., Sheldon, P.J., Bergmann, D.C., et al. (2019). Stem-cell-ubiquitous genes spatiotemporally coordinate division through regulation of stem-cell-specific gene networks. Nat. Commun. *10*, 5574.

45. Langmead, B., and Salzberg, S.L. (2012). Fast gapped-read alignment with Bowtie 2. Nat. Methods *9*, 357–359.

46. Li, H., Handsaker, B., Wysoker, A., Fennell, T., Ruan, J., Homer, N., Marth, G., Abecasis, G., and Durbin, R.; 1000 Genome Project Data Processing Subgroup (2009). The Sequence Alignment/Map format and SAMtools. Bioinformatics *25*, 2078–2079.

47. Cingolani, P., Platts, A., Wang, L.L., Coon, M., Nguyen, T., Wang, L., Land, S.J., Lu, X., and Ruden, D.M. (2012). A program for annotating and predicting the effects of single nucleotide polymorphisms, SnpEff: SNPs in the genome of Drosophila melanogaster strain w1118; iso-2; iso-3. Fly (Austin) *6*, 80–92.

48. Mizuno, S., Osakabe, Y., Maruyama, K., Ito, T., Osakabe, K., Sato, T., Shinozaki, K., and Yamaguchi-Shinozaki, K. (2007). Receptor-like protein kinase 2 (RPK 2) is a novel factor controlling anther development in Arabidopsis thaliana. Plant J. *50*, 751–766.

49. Vermeer, J.E., von Wangenheim, D., Barberon, M., Lee, Y., Stelzer, E.H., Maizel, A., and Geldner, N. (2014). A spatial accommodation by

neighboring cells is required for organ initiation in Arabidopsis. Science *343*, 178–183.

50. Karimi, M., De Meyer, B., and Hilson, P. (2005). Modular cloning in plant cells. Trends Plant Sci. *10*, 103–105.
51. Ossowski, S., Schneeberger, K., Clark, R.M., Lanz, C., Warthmann, N., and Weigel, D. (2008). Sequencing of natural strains of Arabidopsis thaliana with short reads. Genome Res. *18*, 2024–2033.
52. Schwab, R., Ossowski, S., Riester, M., Warthmann, N., and Weigel, D. (2006). Highly specific gene silencing by artificial microRNAs in Arabidopsis. Plant Cell *18*, 1121–1133.
53. Kurihara, D., Mizuta, Y., Sato, Y., and Higashiyama, T. (2015). ClearSee: a rapid optical clearing reagent for whole-plant fluorescence imaging. Development *142*, 4168–4179.
54. Iyer-Pascuzzi, A.S., and Benfey, P.N. (2010). Fluorescence-activated cell sorting in plant developmental biology. Methods Mol. Biol. *655*, 313–319.
55. McKenna, A., Hanna, M., Banks, E., Sivachenko, A., Cibulskis, K., Kernytsky, A., Garimella, K., Altshuler, D., Gabriel, S., Daly, M., and DePristo, M.A. (2010). The Genome Analysis Toolkit: a MapReduce framework for analyzing next-generation DNA sequencing data. Genome Res. *20*, 1297–1303.

STAR★METHODS

KEY RESOURCES TABLE

REAGENT or RESOURCE	SOURCE	IDENTIFIER
Bacterial and Virus Strains		
Escherichia coli DH5α	Thermo-Fisher	Cat# 18265017
Agrobacterium tumefaciens GV3101	N/A	N/A
Chemicals, Peptides, and Recombinant Proteins		
CLE peptides, custom synthesized	GenScript USA	N/A
Brefeldin A (BFA)	Sigma	Cat# 20350-15-6
Estradiol (ES)	Sigma	Cat# 50-28-2
ApaI	Thermo-Fischer	Cat# ER1411
BstBI	Thermo-Fischer	Cat# ER0121
PmeI	Thermo-Fischer	Cat# ER1341
amiRNAs	Thermo-Fischer	N/A
Propidium Iodide (PI)	Invitrogen	Cat# P3566
Calcofluor White M2R	Sigma	Cat# 4359
Critical Commercial Assays		
QIAGEN RNeasy Micro Kit	QIAGEN	Cat# 74004
Clontech SMARTer Ultra Low Input RNA kit v3	Takara	Cat# 634894
Thermoscientific RevertAID First Strand cDNA Synthesis Kit	Termo-Fischer	Cat# K1621
KAPA SYBR FAST qPCR	Sigma	Cat# KK4600
TruSeq DNA NanoSample Prep Kit v2	Illumina	N/A
300cycle high output kit	Illumina	N/A
Experimental Models: Organisms/Strains		
Arabidopsis: Col-0	Widely distributed	N/A
Arabidopsis: *cvp2 cvl1*	[41]	N/A
Arabidopsis: *rpk2-2*	Nottingham *Arabidopsis* Stock Centre	N/A
Arabidopsis: *ops2-2*	[6]	N/A
Arabidopsis: *brx-2*	[42]	N/A
Arabidopsis: *rpk2-2 cvp2 cvl1*	This paper	N/A
Arabidopsis: *rpk2-2 brx-2*	This paper	N/A
Arabidopsis: *rpk2-2 ops-2*	This paper	N/A
Arabidopsis: *bam3-2*	[9]	N/A
Arabidopsis: *socc9 cvp2 cvl1*	This paper	N/A
Arabidopsis: amiRPK2s	This paper	N/A
Arabidopsis: CVP2::NLS-3xVENUS	[4]	N/A
Arabidopsis: CLE45::NLS-3xVENUS	[4]	N/A
Arabidopsis: SMXL3::SMXL3-YFP	[5]	N/A
Arabidopsis: SAPL:: NLS-3xVENUS	This paper	N/A
Arabidopsis: BAM3::XVE::NLS-3xVENUS	This paper	N/A
Arabidopsis: SAPL:: NtdTomato	This paper	N/A
Arabidopsis: NaKR1:: NLS-3xVENUS	This paper	N/A
Arabidopsis: RPK2:: NLS-3xVENUS	This paper	N/A
Arabidopsis: RPK2::XVE::GFP-RPK2	This paper	N/A
Oligonucleotides		
See Table S2	N/A	N/A

(*Continued on next page*)

Continued		
REAGENT or RESOURCE	SOURCE	IDENTIFIER
Recombinant DNA		
pSAPL:: NLS-3xVENUS	This paper	N/A
pBAM3::XVE::NLS-3xVENUS	This paper	N/A
pSAPL:: NtdTomato	This paper	N/A
pNaKR1:: NLS-3xVENUS	This paper	N/A
pRPK2:: NLS-3xVENUS	This paper	N/A
pRPK2::XVE::GFP-RPK2	This paper	N/A
pRPK2::amiRPK2	This paper	See Table S2
pNaKR1::amiRPK2	This paper	See Table S2
pBAM3::amiRPK2	This paper	See Table S2
pCVP2::amiRPK2	This paper	See Table S2
Software and Algorithms		
ImageJ	N/A	https://imagej.nih.gov/ij/
Amira	FEI Visualization Sciences Group	http://www.vsg3d.com/
Cuffdiff	[43]	N/A
Poisson-seq	[44]	N/A
Bowtie2 aligner	[45]	N/A
SAMtools	[46]	N/A
SNPEff tool	[47]	N/A

LEAD CONTACT AND MATERIALS AVAILABILITY

Further information and requests for resources should be directed to and will be fulfilled by the Lead Contact, Antia Rodriguez-Villalon (antiar@ethz.ch). There are no restrictions to the availability of reagents with the exception of custom-made CLE peptides, which will be provided if available.

EXPERIMENTAL MODEL AND SUBJECT DETAILS

Arabidopsis thaliana background lines Columbia (Col-0) were used to perform experiments. Mutants and transgenic lines are in this genetic background as detailed in the Key Resources Table. *Arabidopsis* seedlings were cultivated at 22C under continuous light conditions.

METHOD DETAILS

Plant material and growth conditions

In this study we used previously described reporter lines of *CVP2 [CVP2::NLS-3xVENUS* [4], CLE45 [*CLE45::NLS-3xVENUS* [4]], SMXL3 [*SMXL3::SMXL3-YFP* [31]] and AUX1 [*AUX1::AUX1-YFP* [32]]. Also, mutants *cvp2 cvl1* [41]), *rpk2-2 (*SALK_039514) [48], *ops-2* [6] and *brx-2* [42] were previously described. *Arabidopsis* ecotype Columbia-0 was used as wild-type control in all cases. Seeds were surface-sterilized, stratified at 4°C and grown on 0.5x MS plates under standard continuous-light growth conditions. Chemical treatments were supplemented in the media for indicated concentration and duration of time. CLE peptides were obtained from GenScript USA, while BFA and Estradiol were purchased from Sigma. Prior dilution into media, BFA and Estradiol were dissolved in dimethyl sulfoxide (DMSO), while water was used to dissolve CLE peptides.

Cloning and plant transformation

All constructs were generated using double or triple Multi-Site Gateway system following the handbook instructions. Transcriptional reporters were made as follows: promoter fragments of *RPK2* (1245bp), *SAPL* (1158bp) and *NaKR1* (755bp) were PCR amplified from genomic DNA using the primers described in Table S2. PCR products were introduced via *pDNRP4-P1r* plasmid (Invitrogen) together with *pENzeo-L1-NLS-3xVENUS-L2* into destination vector *pEDO 097* [49]. Alternatively, *SAPL* promotor was recombined with *pENL1-NtdTomato-L2* (obtained from VIB-UGENT) into *pEDO 097*. *BAM3::XVE::NLS-3xVENUS* was generated as follows: *BAM3*^{A} promoter with ATG codon (2142bp) was amplified together with *PmeI/BstBI* sites, latter were used to swap *UBQ10* promoter from *pMDC7*. Ligation was followed by recombination of the pMDC7^{pBAM3} and above mentioned *pENzeoL1-NLS-3xVENUS-L2*. For the purpose of making estradiol inducible expression system under *RPK2* promoter, we first had to expand the amount of available restriction sites of pMDC7, given that *RPK2* promoter contained *BstBI* site. For that purpose, we artificially synthesized DNA

(Thermo Fisher Scientific) containing *PmeI-Multi Cloning Sites (MCS) (ApaI)-BstBI* and first exchange it for *UBQ10* promoter from pMDC7. Then *RPK2* promoter was amplified with *PmeI/ApaI* restriction sites and inserted in modified *pMDC7^{MCS}* in order to obtain *pMDC^{pRPK2}*. Given only one Gateway Site of *pMDC7 attR1-attR2*, we had to perform two step cloning in order to obtain *attL1-GFP-RPK2-attL2*. First, *RPK2* cDNA was amplified with *attB1-attB2* sites and recombined with *pDONR207*. *pEN207 L1-RPK2-L2* was recombined with *pK7WGF2* [50] in order to create *GFP-RPK2* fusion that was again PCR amplified using *GFP_attB1_F* and *RPK2_attB2_R* primers, recombined again into *pDONR207*, and finally into *pMDC7^{pRPK2}* in order to obtain *pRPK2::XVE::GFP-RPK2* construct. To generate *RPK2::RPK2-CITRINE*, *pEN207 L1-RPK2-L2* was recombined with *pEN L4-RPK2-L1r* and *pEN L3-CITRINE-L4* into pH7m34Gw. Finally, for suppressor candidate confirmation and tissue specific *RPK2* silencing, an artificial microRNAs (amiRNAs) was designed by use of WMD3 software [51, 52]. However, *amiRNA* was synthesized (Thermo Fisher Scientific) together with miR319a backbone with *attB1-attB2* sites (full sequence in Table S2), in order to facilitate the creation of *pEN207 L1-ami1/2RPK2-L2*. The latter was used together with tissue specific promoters p*CVP2*, p*RPK2*, p*NaKr1* or p*BAM3^B* in *pEN L4-R1* to recombine into destination *pEDO 097*. p*BAM3^B* promoter differs from *BAM3^A* in lack of ATG start codon. All primers and sequences used for cloning or conformational sequencing were given in Table S2. All constructs were confirmed by sequencing, and transformed through Agrobacterium-mediated transformation into *Arabidopsis* Col-0 plants and/or adequate mutant backgrounds. At least ten independent transgenic lines were analyzed for each construct and the representative one was used for the displayed experiments.

Microscopic analysis and histology

Imaging was performed as previously described [12] using either a Leica SP8 multi-photon or a Zeiss LSM 780 confocal microscopes. In brief, 6-day-old seedlings were stained with propidium iodide (PI, Invitrogen) for live imaging or fixed in 4% paraformaldehyde prior clearing with Clear-See protocol as described in [53] and further stained with Calcofluor White M2R dye (Sigma) prior to visualization. For each image, at least 15 roots were analyzed. For esthetic reasons, images were rotated and displayed on a matching background. All image processing was performed using ImageJ software. Laser ablation of only one dividing protophloem cell per strand (as indicated in text) was performed using the Mai Tai Two Photon laser of the Leica SP8 microscope an EOM at 100% gain was used to limit ablation to a small defined Region Of Interest (ROI) approximately 18 μm^2. Laser output was set at 100% of power with a line averaging of 8X. Following the ablation, protophloem strands were imaged to ensure the ablation was successful (cell-specific) and then seedlings were transferred to MS or CLE45 supplemented media for a 24hr recovery. Seedlings were then fixed with 4% Paraformaldehyde and stained with Calcofluor White to be imaged at Zeiss LSM 780.

CVP2::NLS-3xVenus signal in *cvp2 cvl1* gaps was quantified using ImageJ and calculated by formula: Corrected Total Nuclear Fluorescence = Integrated Density – (Area of selected nucleus x Mean fluorescence of background readings). Gap fluorescence is always calculated as percentage of the closest thick-cell-walled cell signal. The average was made from all gap cells from 20 seedlings.

SBFSEM

6-day-old roots were stained for 5 min in a 10 μg/ml aqueous solution of propidium iodide and visualized with the confocal laser-scanning microscope as previously described. Roots displaying gap cells were selected and prepared for SBFSEM according to [8]. For SBFSEM, a FEI Quanta 250 (Thermo Fisher Scientific) with integrated 3view ultramicrotome (Gatan) was used. The block face was cut with 200 nm increments. Images were processed and visualized in Amira (FEI Visualization Sciences Group). Protophloem strands were identified according to their position within the root stele.

FACS, RNA isolation and RNA library preparation

Fluorescence activated cell sorting (FACS) of *CVP2::NLS-3xVENUS* protoplasts were performed as previously described [44, 54]. In short, 0.3 cm of the root tips from 5-day-old *cvp2 cvl1* and Col-0 plants harboring *CVP2::NLS-3xVENUS* construct were used as starting material for protoplasting and FACS. Upon sorting, total RNA was extracted by use of QIAGEN RNeasy Micro Kit, and quality control was performed on Bioanalyzer (RIN > 7). RNA that passed quality control was further used for cDNA synthesis by use of PolyA primers and Clontech SMARTer Ultra Low Input RNA kit v3. cDNA was amplified using the same kit. Next-generation sequencing was performed with Hiseq 2500 Machine in quadruplicates, and reads were mapped back to the genome. Differential gene expression was analyzed using Cuffdiff [43] or with Poisson-seq pipeline.

RNA isolation and quantitative RT-PCR

RNA from whole seedlings was extracted using the QAGEN RNeasy Plant Micro kit following manufacturer's instructions. 1ug of total RNA was used to prepare Poly(dT) cDNA using Thermoscientific RevertAID First Strand cDNA Synthesis Kit following manufacturer's instructions. qPCR was carried out using KAPA SYBR FAST qPCR mix and following the manufacture's protocol. All reactions were performed in triplicates and using the indicated pair of genes with IPP2q_F and IPPq_R as housekeeping genes (Table S2). Signals were normalized using housekeeping genes while data analysis was performed utilizing the Second Derivative Maximum Method.

EMS mutagenesis, DNA extraction, library preparation and Next Generation Sequencing

EMS mutagenesis on *cvp2 cvl1* seeds was performed using standard methods procedures. M2 pools of around 100 seedlings each were screened selecting only the long rooted ones compared to the short rooted control *cvp2 cvl2* at 7dag and transplanted in soil.

After genotyping for *cvp2* and *cvl1* homozygosity, the progeny of these plants were rescreened in the M3 generation analyzing protophloem continuity. Seedlings were grown on MS plates for 7days under continuous light conditions. To map the mutations responsible for *cvp2 cvl1* suppressing phenotype we extracted genomic DNA from entire seedlings that were pooled from the F2 segregating population of the backcrossed suppressors to *cvp2 cvl1.* Genomic DNA extraction was done using cetyltimethyl ammonium bromine (CTAB) 2% buffer with 1% Polyvinylpyrrolidone (PVP) and samples were resuspended in 30ul H_2O. The TruSeq DNA NanoSample Prep Kit v2 (Illumina, California, USA) was used for library creation with starting material of 1 μg fragmented DNA that was sonicated to fragment size of 550bp. Size selection of the fragmented DNA samples was done using AMpure beads, end-repaired and polyadenylated. Following, TruSeq adapters containing the index for multiplexing were ligated to the fragmented DNA samples. Selective PCR enrichment of the fragments containing TruSeq adapters on both ends was completed and the quality and quantity of the enriched libraries was validated using Qubit (1.0) Fluorometer and the Tapestation (Agilent, Waldbronn, Germany). The libraries were normalized to 10nM in Tris-Cl 10 mM, pH8.5 with 0.1% Tween 20. Sequencing was completed at the Functional Genomics Center at ETH Zurich and performed using the Illumina Nextseq 500 system with the 300cycle high output kit. (Illumina, Inc, California, USA). Reads were quality-checked with fast quality control to measure various quality metrics for the raw reads. Sequence reads were mapped to the TAIR10 *Arabidopsis thaliana* genome using the bowtie2 aligner (v. 2.3.1, parameter–end-to-end [45]. Alignment files were converted from SAM (Sequence Alignment/Map) format to BAM with SAMtools (v 1.8 [46]). SNPs calling was performed using the GATK tool (v. 4.1.0.0 [55]). Background SNPs (found in the *cvp2 cvl1* parental line) were filtered out from putative target SNPs using the intersectBed tool from the BEDTools utilities (v. 2.22.1). Remaining putative target SNPs were filtered for read depth (at least 10X) using vcftool from SAMtools. The SNPEff tool (v 2.0.4 RC1 [47]) was used to predict the effect of the SNPs in coding regions. An in-house script was used to extract the SNP frequencies (the number of reads supporting a given SNP over the total number of reads covering the SNP location) which were then plotted with R (v 3.6). The causal mutation was isolated by selecting the SNPs expected to be induced by the mutagenesis having a frequency of 70% or higher in our suppressors versus less than 50% in the *cvp2 cvl1* parental line.

QUANTIFICATION AND STATISTICAL ANALYSIS

In all plots, error bars represent standard errors (SE) and n represents the number of samples analyzed when relevant. The statistical analysis performed in each case is indicated above each plot. Pairwise comparisons among multiple samples was performed using a one-way ANOVA analysis with post hoc Tukey HSD testing. Significantly different groups (p value indicated within the plot) of samples are indicated using lower case letters. When indicated, Fisher's test of independence was employed to analyze the differences between two different groups. Significantly differences ($p < 0.05$) are indicated with an asterisk. The significantly differences between WT and cvp2 cvl1 expression of the genes listed in Figure S1C and Table S1 was calculated using standard tow-sided Student t testing. * indicates a p value < 0.05 and ** indicates a p value < 0.01 and *** indicates a p value < 0.001.

DATA AND CODE AVAILABILITY

The published article includes all transcriptome dataset (Table S1) generated during this study.